Journal of Applied Polymer Science

Structure–property relationship of sodium deoxycholate based poly(ester ether)urethane ionomers for biomedical applications

Daniela Filip,[1] Doina Macocinschi,[1] Stelian Vlad,[1] Gabriela Lisa,[2] Mariana Cristea,[1] Mirela F. Zaltariov[1]

[1]Petru Poni Institute of Macromolecular Chemistry, Aleea Grigore Ghica Voda 41 A, Iasi 700487, Romania

[2]Chemical Engineering Department, Faculty of Chemical Engineering and Environmental Protection, Gheorghe Asachi Technical University, Bulevardul Dimitrie Mangeron 73, Iasi 700050, Romania

Correspondence to: D. Filip (E-mail: dare67ro@yahoo.com)

ABSTRACT: New sodium deoxycholate based poly(ester ether)urethane ionomers were prepared for the development of biomedical materials. A structure–property relationship in the tested biomaterials was established by cross-examination of the dynamic mechanical and dielectric properties, attenuated total reflection–Fourier transform infrared investigation, thermogravimetric analysis, and surface morphology characterization. A stronger ionic interaction and solvation capacity of the ions and a higher ionic conductivity were manifested in the case of poly(ethylene oxide)-rich segments than for poly(propylene oxide)-rich segments in these polyurethane ionomers. The molecular and ionic interactions of the bile-salt moiety with different polyether cosoft segments influenced chain packing and conformation, supramolecular organization, and the resulting surface morphological microstructures of the polyurethane biomembranes. © 2015 Wiley Periodicals, Inc. J. Appl. Polym. Sci. **2016**, *133*, 42921.

KEYWORDS: biomaterials; polyurethanes; thermogravimetric analysis (TGA)

Received 12 June 2015; accepted 5 September 2015

DOI: 10.1002/app.42921

INTRODUCTION

Polyurethanes are characterized by structure–property versatility and represent one of the most biocompatible and hemocompatible materials applied for the development of medical devices.[1–3] Also, they are characterized by a propensity for bulk and surface modification by the use of a hydrophilic–hydrophobic balance[4,5] or by the attachment of biologically active species via chemical groups distinctive for their polyurethane structure. These innovative technical approaches have been used to obtain functional devices that behave like natural tissue.[6] Numerous reports in the literature deal with the biocompatibilization or functionalization of polyurethanes.[7] The biological response of polyurethanes can be improved by means of conjugation, blending, or coating with natural polymers.[8,9] The modification of the polymers has also been considered also for reducing infections caused by biomedical devices.[10,11]

Bile acids are natural-origin steroidal compounds metabolically synthesized from cholesterol in the liver and stored in the gall bladder. Sodium deoxycholate (SD) is at present used for biomedical and supramolecular applications.[12] Bile acids confer biocompatibility, a high stability of the steroid skeleton, facial amphiphilic characteristics, chirality and a self-assembly capacity when attached to polymers.[13,14] Because bile acids are naturally occurring compounds, they have drawn attention in the synthesis of polymers for biomedical and pharmaceutical applications.[15–18] Various types of polyurethane ionomers are used as solid polymer electrolytes because of their good chemical stability, excellent mechanical properties, and low glass-transition temperature (T_g) values, and they are also used as biomedical products.[19–21] Polyurethane ionomers based on poly(ethylene oxide) (PEO) have been investigated for both their good mechanical strength and high ionic conductivity. Polyurethane is an attractive material because it possesses both a mechanically strong hard phase and a fast-relaxing soft phase, which can potentially have a high conductivity. A low-molar-mass carboxylate diol is used to prepare carboxylate-based polyurethane ionomers, and this places the carboxylate groups in the hard segment. It is very well known that poly(ester urethane)s possess superior mechanical properties and better resistance to oxidation compared to poly(ether urethane)s. Conversely, poly(ether urethane)s exhibit better hydrolytic stability and functionality at low temperatures. Mixtures of polyester and polyether polyols have been used in the synthesis of the polyurethanes with adapting degradation and hydrophilic–hydrophobic properties.

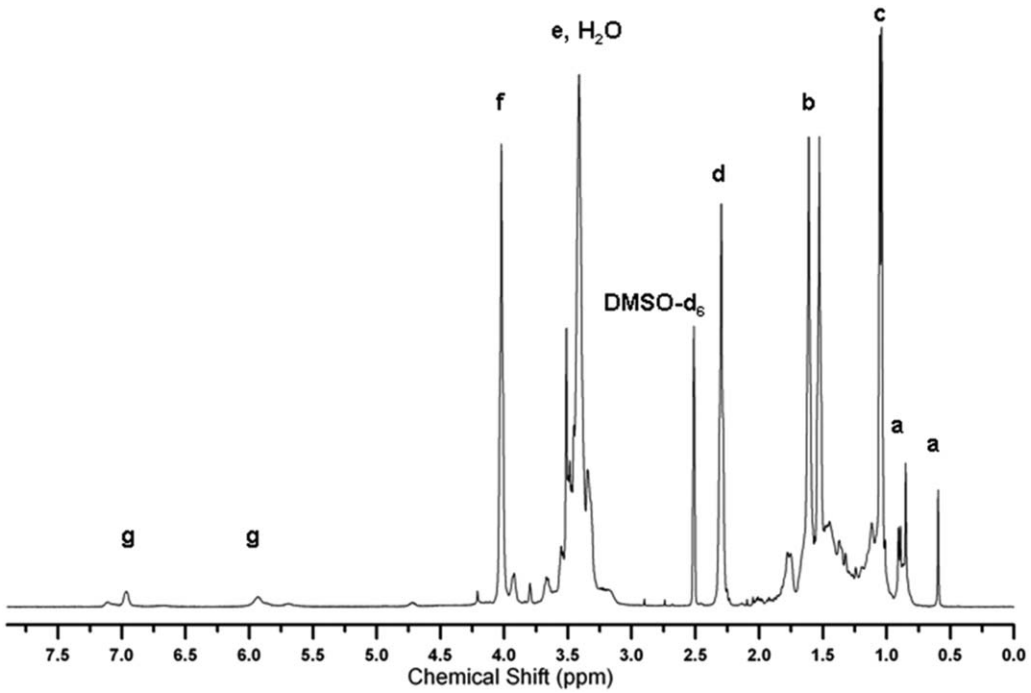

Figure 1. ^{1}H-NMR spectrum (DMSO-d_6) of the P1 polyurethane.

In this study, new poly(ester ether)urethanes based on SD as a chain extender were examined. The applications of thermal analyses, such as differential scanning calorimetry (DSC), dynamic mechanical thermal analysis (DMTA), and dielectric thermal analysis (DETA), to the fields of biomaterials made valuable contributions to their structural and conformational determinations.[22,23] Thermogravimetry (TG) and derivative thermogravimetry (DTG) under dynamic conditions of temperature and the evaluation of the corresponding kinetic parameters were also used to analyze the biomaterials and to measure the mass loss, thermal decomposition, and thermal stability and investigate the degradation mechanisms. The purpose of this study was to evaluate the morphology, ionic conductivity, and thermal, dynamic mechanical, and dielectric properties to investigate the structure–property relationships of these synthesized bile-salt-based poly(ester ether)-urethane ionomers.

EXPERIMENTAL

Materials

Poly(ethylene glycol) (PEG)-*block*-poly(propylene glycol)-*block*-PEG (Pluronic L31-PL31) was purchased from Sigma-Aldrich [PEO_2 $PPO_{16}PEO_2$; number-average molecular weight (M_n) = 1100 g/mol (Pluronic L31)]. Poly(ethylene glycol-*ran*-propylene glycol) (PEO-ran-PPO) with 25 wt % PPO units was purchased from Sigma-Aldrich (M_n = 2500 g/mol). PEG was purchased from Sigma-Aldrich (Germany, M_n = 2000 g/mol). Poly(propylene glycol) (PPG) was purchased from Fluka Chemie GmbH (Switzerland, M_n = 2000 g/mol). Poly(butylene adipate)diol (PBA) was purchased from Sigma-Aldrich (United Kingdom, M_n = 2000 g/mol). SD was purchased from Sigma-Aldrich (New Zealand) and were used as received. Methylene dicyclohexyl diisocyanate (H_{12}MDI) was purchased from Sigma-Aldrich and was used as received. Four different polyurethanes, P1 [(PL31 + PBA)/H_{12}MDI/SD], P2 [(PEO-*ran*-PPO + PBA)/H_{12}MDI/SD], P3 [(PEG + PBA)/H_{12}MDI/SD], and P4 [(PPG + PBA)/H_{12}MDI/SD] were prepared by a typical two-step solution polyaddition with *N,N*-dimethylformamide (DMF, Fluka P.A., Germany) as a solvent. First, the NCO-terminated prepolymer was prepared by the dehydration of a 1:1 mixture of polyester (PBA) and polyether for 3 h at 90°C *in vacuo* followed by the addition of H_{12}MDI to the vigorously stirred macrodiol. The amounts of diisocyanate and macrodiol were kept at a molar ratio of 2:1. The reaction between the diisocyanate and macrodiol took place for 2.5 h under a nitrogen atmosphere at 80°C in the presence of dibutyltin dilaurate (95%, Aldrich) as a catalyst. The temperature was lowered to 70°C, and the chain extender SD was added. The reaction continued for 2 h. The resulting polymers were precipitated in water and dried *in vacuo* for several days. Characteristic assignments were found by attenuated total reflection (ATR)–Fourier transform infrared (FTIR) spectroscopy and ^{1}H-NMR [hexadeuterated dimethyl sulfoxide (DMSO-d_6)] analyses. For example, the ATR–FTIR spectrum of the polyurethane P1 showed the following signals: 3430–3200 cm^{-1} (>NH stretching), 3019–2765 cm^{-1} (aliphatic groups), 1729 cm^{-1} (carbonyl stretching of ester and urethane groups), 1546 cm^{-1} (—COO^- stretching), and 1224–1000 cm^{-1} (—C—O—C— stretching). In Figure 1, the ^{1}H-NMR spectrum (DMSO-d_6) of the polyurethane P1 is shown and includes the following peaks: (a) δ = 0.6, 0.82, and 0.87 ppm (methyl protons of SD); (b) δ = 0.98–2.0 ppm (steroidal protons); (c) δ = 1–1.2 ppm (H_{12}MDI and PL31 methyl protons); (d) δ = 2.3 ppm —CH_2—CO—; (e) δ = 3.1–3.7 ppm [—CH_2—CH_2—O— (PEO) and >CH—CH_2—O— (PPO) protons]; (f) δ = 4 ppm (—CH_2—O—CO—; and (g) δ = 5.7–7.2 ppm (—NH— of urethane groups).

The chemical synthesis route of the studied poly(ester ether)urethane ionomers is presented in Scheme 1.

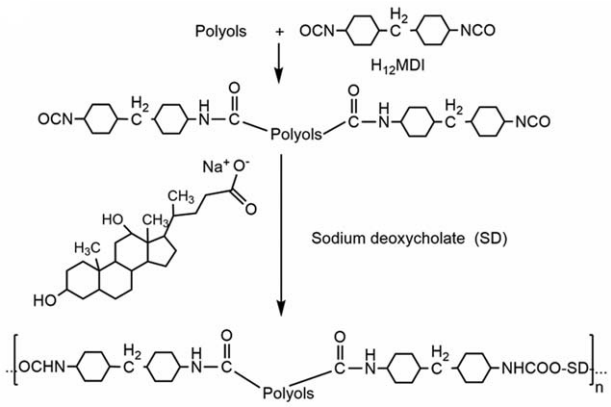

Scheme 1. Chemical synthesis route of the studied poly(ester ether) urethane ionomers.

Preparation of the Poly(ester ether)urethane Ionomer Film Samples

The poly(ester ether)urethane ionomer film samples were prepared by a solvent-casting method (polyurethane solutions in DMF, 40 wt %). The solvent was evaporated in an oven under circulating air for several hours and afterward in a vacuum oven for several days. All of these films were used for the research investigations presented in this article.

Measurements

The ATR–FTIR spectra were recorded with an FTIR Bruker Vertex 70 spectrometer equipped with a ZnSe crystal. The spectra were recorded in ATR mode in the 600–4000-cm^{-1} wavenumber range at room temperature (RT) with 32 scans per spectrum at a resolution of 4 cm^{-1}. Temperature-dependent ATR–FTIR spectra were recorded during heating runs on the same instrument equipped with a Golden Gate single-reflection ATR accessory and a temperature controller. The solid sample was added to the ATR crystal surface. The temperature varied between 30 and 190°C and was increased by 20°C at each measurement. After the temperature was changed, the sample was maintained for 2 min before the spectrum was acquired. The spectroscopic manipulation, which included baseline correction, normalization, and peak areas results, were performed with the OPUS 6.5 software package. The overlapped and hidden peak positions of the experimental spectra were determined with the second derivative of the spectra. The C=O stretching vibration region was deconvoluted by a curve-fitting method, and the areas were calculated with a 50% Lorentzian + 50% Gaussian function. The curve-fitting analysis was performed with the OPUS 6.5 software. The procedure led to a best fit of the original curve with an error of less than 0.002.

^{1}HNMR spectra were obtained with a Bruker Avance DRX 400 instrument (DMSO-d_6).

The molecular weight was determined with a GPC PL-EMD 950 evaporative mass detector instrument with conventional calibration with polystyrene standards (solution in DMF, 1 wt %).

A Mettler-Toledo DSC 1 apparatus operating under nitrogen with a heating–cooling rate of 10°C/min, a range of investigated temperatures of −90 to 190°C, a nitrogen flow of 150 mL/min, and a sample weight of 5–7 mg was used for the thermal analysis of the polyurethane samples.

DMTA experiments were performed with a PerkinElmer Diamond instrument that applied a sinusoidal stress to the sample and measured the resulting strain. The force amplitude used was well within the linear viscoelastic range for all of the investigated samples. The thermomechanical properties were evaluated at a heating rate of 2°C/min in a multiplex experiment (at 0.5, 1, 2, 5, and 10 Hz) under a nitrogen atmosphere. The range of investigated temperatures was from −150 to 100°C. Variations in the storage modulus (E'), loss modulus (E''), and tension loss tangent (tan δ) as a function of the temperature were obtained.

The dielectric measurements were carried out with a Novocontrol system Concept 40 broadband dielectric spectrometer (Germany) equipped with an Alpha Frequency Response Analyzer and a Quatro temperature controller. A heating rate of 5°C/min over the temperature range from −150 to 80°C was used, and 7 decades of frequency (f = 10–10^6 Hz) were scanned. The samples for the dielectric measurements consisted of films with thicknesses in the range 15–25 μm placed between two flat round electrodes 20 mm in diameter. The amplitude of the applied voltage was 1 V.

The thermal stability of the polyurethanes was examined on a DERIVATOGRAF Q-1500 D apparatus (Hungary). The rate of the thermogravimetric analysis scans was 10°C/min in an air atmosphere. The initial weight of the samples was about 50 mg, and the temperature range was 30–700°C.

Scanning electron microscopy (SEM) analysis was performed with a Quanta 200 scanning electron microscope with an integrated EDS system, a Genesis XM 2i EDAX with an SUTW detector. The magnification is indicated on the micrographs.

RESULTS AND DISCUSSION

ATR–FTIR Spectroscopic Characterization of Hydrogen Bonding

Supramolecular chemistry takes care of intermolecular interactions, that is, noncovalent interactions, such as metal-ion coordination, electrostatic forces, hydrogen bonding, donor–acceptor interactions, van der Waals interactions, and secondary bonds realized between building blocks for molecular assemblies. Hydrogen bonding is very important for the supramolecular architecture of polyurethanes. In general, poly(ester ether)urethanes are characterized by hard–hard-segment hydrogen bonding (NH—O=C) and hard–soft-segment hydrogen bonding involving ether oxygen (NH—O) or ester carbonyl (NH—O=C), which represent the extent of phase mixing of the hard–soft phase. It is usually accepted that a major factor in phase separation is the strong hydrogen bonding between urethane-type hard segments and/or hard-segment crystallization. Carbonyl stretching bands are characterized by multiple separate individual carbonyl absorptions, which reflect the complex properties of hydrogen bonding in the polyurethanes at higher wavenumber bands attributed to free urethane and ester carbonyls,

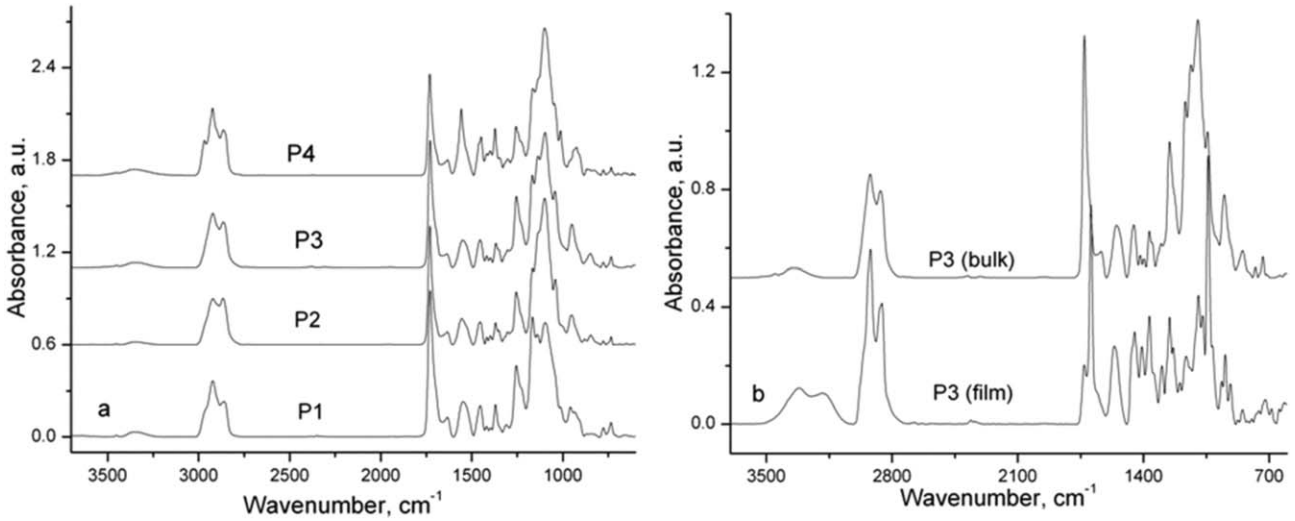

Figure 2. ATR–FTIR spectra of the (a) synthesized poly(ester ether)urethane ionomers (bulk samples) and (b) P3 bulk and film samples.

as reported in other articles,[24,25] and at lower wave-number bands attributed to hydrogen-bonded carbonyl groups in ordered (crystalline domains) and disordered (amorphous domains) domains. More or less ordered or disordered interfacial domains in the poly(ester ether)urethane matrix, which reflect the level of each of the morphological regions, were found.

In Figure 2, the ATR–FTIR spectra of the synthesized poly(ester ether)urethane ionomers bulk samples [Figure 2(a)] and the bulk and film samples of P3 [Figure 2(b)] are presented.

We found that for polyurethanes with higher PEO (hydrophilic)–PPO (hydrophobic) ratios, that is, P2 and P3, significant spectral changes were recorded when the bulk (polyurethanes obtained from synthesis) and film samples (solvent-cast samples in DMF) were compared. Directional intermolecular forces, as in the case of solvent-cast samples, induced self-assembly and self-organization.

In the ATR–FTIR spectra [Figure 2(b)], the characteristic absorbance bands, including those at 2870–2918, 1410–1468, and 721–735 cm^{-1}, were assigned to the symmetrical and asymmetrical stretching, bending, and rocking vibrations of methylene groups, whereas those at 1691–1730 cm^{-1} were attributed to the stretching vibrations of the C═O bond. The spectra of the same sample in bulk and in the film were different. This was attributed to the different arrangement of the polymeric chains in bulk and in the film. An important factor that determined these changes was the higher hydrophilicity and flexibility of the polymeric chains; this was due to the different packing motif in the bulk and film. The observed changes included an increase in the absorbance band in the region 3000–3400 cm^{-1} in the film; this was assigned to the NH groups. In this region, there were two strong bands at 3315 and 3188 cm^{-1}, whereas in the ATR–FTIR spectrum of the bulk, a broad band was present. This was assigned to the intermolecular H bonding between the C═O and N—H groups.[26] Other changes occurred in the 1730–1690-cm^{-1} region that were due to C═O stretching vibrations from urethane and ester bonds. The carbonyl region is usually used to describe the hydrogen-bonding interactions of poly(ester urethane) ionomers. In this region, two absorption bands occurred: one that was due to nonassociated (free) urethane and ester (1730 cm^{-1}) and another one that was due to the hydrogen-bonded groups (1691 cm^{-1}).[24,25] The differences consisted of the decrease in the band at 1730 cm^{-1} in the film in comparison with that of the bulk. Such a decrease in the C═O stretching vibration obviously indicated the modification of hydrogen bonds: C═O…N—H. At the same time, the increase in the band at 1691 cm^{-1} in the film as compared to the bulk was also characteristic of intermolecular H bonds. The presence of the deoxycholate anion in the structure was evidenced by the bands at 1562 and 1410 cm^{-1} (in the film) and 1543 and 1398 cm^{-1} (in the bulk); these were attributed to asymmetric and symmetric stretching vibrations of COO^-, respectively. The amide I band appeared at 1637 cm^{-1} in the bulk and at 1655 cm^{-1} (as a shoulder) in the film, whereas the amide III, due to C—N—H group vibrations, overlapped with those of the carboxylate ones. Other changes included an increase in the absorbance of the band at 1366 cm^{-1} in the film because of the symmetrical bending of C—H bonds in methyl groups and bands at 1452–1468 cm^{-1} due to the bending vibrations of C—H bonds in methylene groups. The higher ordered structures resulted from the association of the amphiphiles showing an increase in absorbance. In the 1000–1200-cm^{-1} region, the bands at 1041 and 1067 cm^{-1} in the film were attributed to C—O stretching and cyclohexane ring vibrations and were well defined as compared with those in the bulk, where the bands overlapped with those specific to the C—C skeletal vibrations and C—O stretching of ester groups.[27]

The deconvoluted IR spectra and the curve-fitting results of the C═O stretching region recorded at 30, 90, and 190°C of the P1 and P2 bulk and film samples are shown in Figure 3 and Table I, respectively. The study of the carbonyl stretching region revealed the presence of three different bands attributed to the increasing f to ordered and disordered H-bonded C═O and non-hydrogen-bonded C═O groups. As the temperature rose, the carbonyl bands shifted slightly to higher fs. At 190°C, the carbonyl stretching region was resolved only into two different

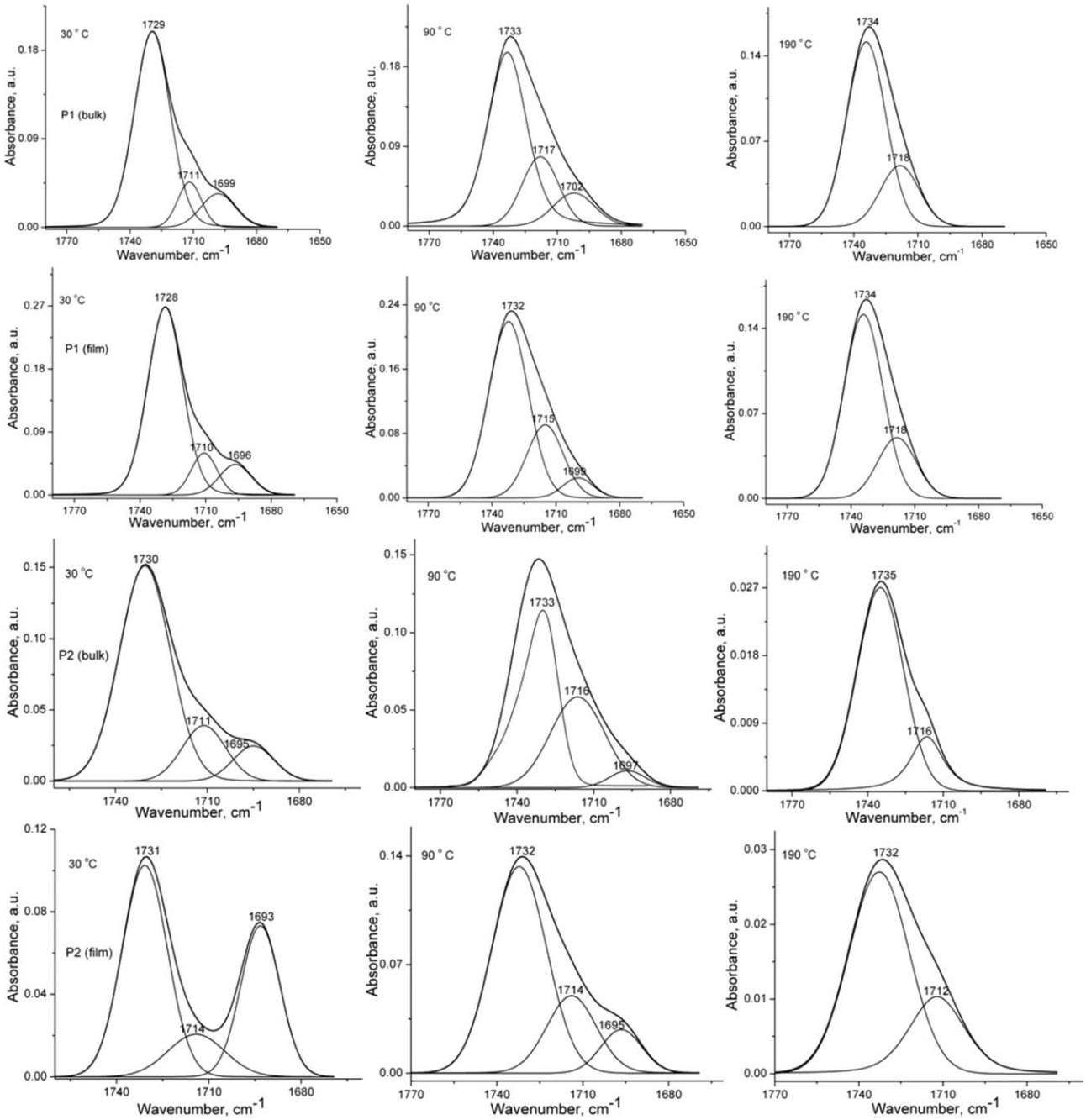

Figure 3. Deconvoluted IR spectra of the C═O stretching region recorded at 30, 90, and 190°C for the P1 and P2 bulk and film samples.

bands. The areas of the ordered H-bonded C═O groups in both the film and bulk samples decreased as the temperature increased; this suggested a loss of order.

The energy of hydrogen bonds (E_H) corresponding to the N—H stretching vibrations region was calculated with the following equation:[28]

$$E_H = \frac{1}{k}\frac{v_0 - v}{v_0} \quad (1)$$

where v_0 is the monomeric N—H stretching frequency located at 3474 cm^{-1}, v is the stretching frequency of the H-bonded N—H groups in the FTIR spectra of the analyzed samples, and k is a constant ($1/k = 2.625 \cdot 10^2$ kJ). With the Sederholm equations,[29] the R_s in equation (2) and Table II were calculated as follows:

$$\Delta v\left(cm^{-1}\right) = 548(3.21 - R_s) \quad (2)$$

where $\Delta v = v - v_0$. The E_H and R values for the analyzed samples are shown in Table II.

These results show stronger interactions between the macromolecular chains, lower hydrogen-bond distances, and increased chain packing for the P2 and P3 film samples.

Table I. Curve-Fitting Results in the Range 1800–1600 cm^{-1} for the Bulk and Film Samples of P1 and P2

	Ordered/disordered hydrogen-bonded C=O (cm^{-1}) and area value				Free C=O (cm^{-1})			
Temperature (°C)	P1 film	P1 bulk	P2 film	P2 bulk	P1 film	P1 bulk	P2 film	P2 bulk
30	1696/1710	1699/1711	1693/1714	1695/1711	1728	1729	1731	1730
Area	0.79/0.87	0.69/0.64	1.16/0.47	0.41/0.68	5.53	4.38	1.88	3.12
90	1699/1715	1702/1717	1695/1714	1697/1716	1732	1733	1732	1733
Area	0.43/1.92	0.90/1.67	0.5/1.1	0.19/1.55	5.07	5.11	3.18	2.98
190	—/1715	—/1718	—/1712	—/1716	1734	1734	1732	1735
Area	—/0.75	—/1.13	—/0.29	—/0.15	3.5	3.45	0.72	0.62

DSC Measurements

The thermal transitions in the polyurethanes were directly related to the degree of phase separation between the hard and soft segments. DSC thermograms of the studied polyurethane ionomers P1–P4 reveal only one T_g; this showed phase segregation between the mixed polyester (more rigid)–polyether (more flexible) soft phase and the phase-segregated hard phase. The T_g values and corresponding change in heat capacity (Δcp) values are shown in Table III. The T_g values were influenced by the polyurethane network, which restricted the mobility of the soft-segment units. The presence of ionic groups affected the hydrogen-bonding interactions. In general, ionomers can develop specific interactions with various polar groups, and this enhances the compatibility. For example, ionic interactions are found to favor the compatibility of polyester ionomers with poly(ethylene terephthalate) and nylon 6.[30] Because of the strong interaction of the PEO segments with both the urethane linkages and ions, the hard–soft phase mixing and fewer ion aggregates were favored. In Figure 4, the DSC thermograms (second heating run) of the studied polyurethane ionomers P1–P4 are presented. For polyurethane P3, which contained PEO as a cosegment, the DSC thermogram (second heating run) revealed a melting temperature (T_m) of 34.3°C and a cold crystallization peak at a crystallization temperature of 7.0°C. For polyurethanes P1, P2, and P4, the T_ms vanished during the second heating runs. With its short polyether segment and a higher content of hard segment, the T_g of P1was found to be higher than that found for the polymer with a long polyether segment and a lower content of hard segment (P2). For the same content of hard segment, the more crystalline PEO segment (P3) induced a higher T_g than that of P4, which contained more amorphous PPO segment.

DMTA

With DMTA methods, the thermomechanical properties of polymers can be measured. When the structures of the polymers are more complex, the difficulty in interpreting the results is increased,[31] mostly because there are overlapping phenomena whose effects sometimes balance out. The glass transition is readily identified from a sharp drop in E', E'', or tan δ. The criteria for the selection of T_g from DMTA is the peak E'' or peak tan δ. T_g increases with f because as the test f increases, the relaxations associated with the glass transition can occur at higher temperatures.

The drop in E' represents the onset of long-range molecular motions (α relaxation), a phenomenon that is attributed to the glass transition. When the decrease in E' is small (which is also associated with a low tan δ peak), there are constraints, such as crystalline domains or chemical–physical crosslinks, that impede the free movement of the amorphous segments. Also, the E' descent is less steep (large tan δ peak) for inhomogeneous structures. In Figure 5(a), the isochronous curves (at 1 Hz) of the E' values of samples P1–P4 are presented. We found the following order for the glassy-state modulus in the studied polyurethane samples: P3 > P4 > P2 > P1. The soft-segment crystallinity enhanced the low-temperature stiffness of the polyurethanes. The crystalline regions of the soft domain contributed to the mechanical integrity of the polyurethanes. PPO segments decreased the crystallinity and thus decreased the stiffness of the material. The PEO–PPO ratio had a strong influence on the dynamic behavior and morphological structure of the studied polyurethanes.

All of the polyurethanes (P1–P4) showed an E' drop during the glass transition that was less than three orders of magnitude because of the semicrystalline nature and the hydrogen bonds inside the hard domains and/or between the hard and soft domains. The soft blocks, having various tendencies to crystallize and phase-segregate, were capable of generating multiple levels of ordering with the unique energy-absorbing properties of natural materials.[32,33] For the polyurethane P1, maybe the low molecular weight of Pluronic L31 determined the value of E' in the glassy region to be under 10^9 Pa. Because the descent

Table II. Energy and Distance Values of the Hydrogen Bonds for the Analyzed Polyurethane Samples

	P1 film	P1 bulk	P2 film	P2 bulk	P3 film	P3 bulk	P4 film	P4 bulk
E_H (kJ)	12.5	18.6	21.9	18.6	21.6	11.5	12.9	12.1
R_s (Å)	2.90	2.76	2.68	2.76	2.68	2.93	2.89	2.91

Table III. Molecular Weights, Dispersity Indices, and Thermal Characteristics from DSC

Sample	M_n	M_w/M_n	T_g (°C)[a]	Δcp (J g^{-1} K^{-1})[a]
P1	30,551	1.281	−47.2	0.40
P2	30,898	1.300	−59.4	0.55
P3	49,152	1.288	−51.9	0.53
P4	29,500	1.258	−56.4	0.44

M_w, weight-average molecular weight.
[a] From the second heating run.

of E' took place in steps, there were segregated domains. As shown, polyurethanes P3 and P2 showed E' curves typical of a phase-segregated structure by revealing the glass transitions of the hard segments, which are melting phenomena related to the soft and hard segments, and polyurethanes P1 and P4 behaved like homogeneous polymeric networks. In Figure 5(b), the isochronous curves (at 1 Hz) of the loss dispersion (E'') of P1–P4 are presented. They evidence the main α mechanical relaxation and secondary relaxations for polyurethanes P1–P4, and the values of the transition temperatures are tabulated in Table IV.

In Figure 5(c), the isochronous curves (1 Hz) of the tan δ of P1–P4 are presented. They reveal the glass transition and secondary relaxations. The height and shape of the tan δ peaks corresponding to the T_g values reveal the degree of order and freedom of molecular mobility of the soft segment. For polyurethane P1 (shorter polyether cosoft segment, $M_n = 1100$ g/mol), the strong interaction of ester groups made the segmental mobility difficult at T_g. It was very evident in the case of P1 that the tan δ peak had only an ascending side, which was followed not by a descending side but by a large plateau. The elongation of the samples was less than 5% during melting; after this process, the samples were still load-bearing. The melted segments functioned as plasticizers for the hard phase, accelerating its relaxation. Because of the high mobility, longer polymer segments started to slip one past another; this determined the rapid increase in tan δ. Because of the structural features of P3, we had no doubt that it had the strongest hydrogen-bonding network. The temperature at which tan $\delta = 1$ (E'' becomes higher than E') was the highest at 81°C (P3 sample).

DETA

The dielectric relaxation spectroscopy technique is of individual interest because of its wide f range and its capability of following the reorientational motions of dipolar groups, polymer chain segments, or whole molecules. The supramolecular architecture of these polyurethanes involves both self-assembly and ion recognition. For PEO-based polyurethane ionomers, the ionic groups have favorable interactions with the polymer matrix. Generally, the ionic groups can facilitate the formation of ionic aggregates, which act as physical crosslinks. The states of ions are influenced by the PEO segment length and also by the temperature. The solvation capacity of ions of PEO in comparison with PPO is linked to the preference of PEO for the gauche state about the constituent OC—CO bond, whereas the side methyl group in PPO sterically hinders this conformation.[34]

In Figure 6, the isochronous curves (at 1 Hz) of the real and imaginary parts of the complex dielectric permittivity, tan δ, and conductivity of the polyurethane ionomer samples P1–P4 are shown.

Polyurethane P2 showed similar behavior to P3, and polyurethane P1 showed similar behavior to P4. This could be explained by the strong influence of the PEO–PPO ratio on the solvation capacity of the ions, which dictated the dielectric relaxation thermal behavior of the studied polyurethane ionomers P1–P4. From low to high values of real part of permittivity (ε') with increasing temperature, the steplike transition was evident in the variation of the dielectric properties of the investigated polyurethanes. These transitions were connected with the relaxation processes, which were accompanied by loss peaks or shoulders in the diagrams of dielectric loss (ε'') or tan δ versus temperature for the studied polyurethanes P1–P4. The moisture content can be a significant factor affecting polymer relaxations.[35] For P1 and P4, the ε'' curves showed the α dielectric relaxations as shoulders because of the contribution of conductivity and secondary relaxations at lower temperatures. For P2 and P3, the ε'' curves showed that the α dielectric relaxation was a minor event that was strongly overlapped by the conductivity contribution, and they showed secondary relaxations at lower temperatures. For a f of 1 Hz at temperatures higher than the T_g values, both ε' and ε'' increased with increasing temperature because of the increasing conductivity. Large loss factors in the polymers were obtained when the temperature was above the glass transition because of the ionic conduction contribution to the loss factor. In Figure 6(c), the isochronous curves (at 1 Hz) of the tan δ values of P1–P4 are presented. Strong conductivity relaxation peaks were observed for polyurethanes P1–P4 at temperatures higher than T_g. For P2 and P3, the α dielectric relaxation was a minor event that was strongly overlapped by the conductivity contribution, whereas for P1 and P4, the α dielectric relaxation was revealed as shoulders because of the contribution of conductivity, and at higher temperatures,

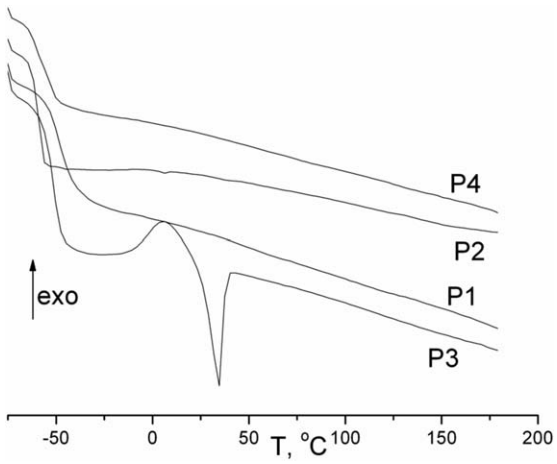

Figure 4. DSC thermograms (second heating run) of the P1–P4 poly(ester ether)urethane ionomers.

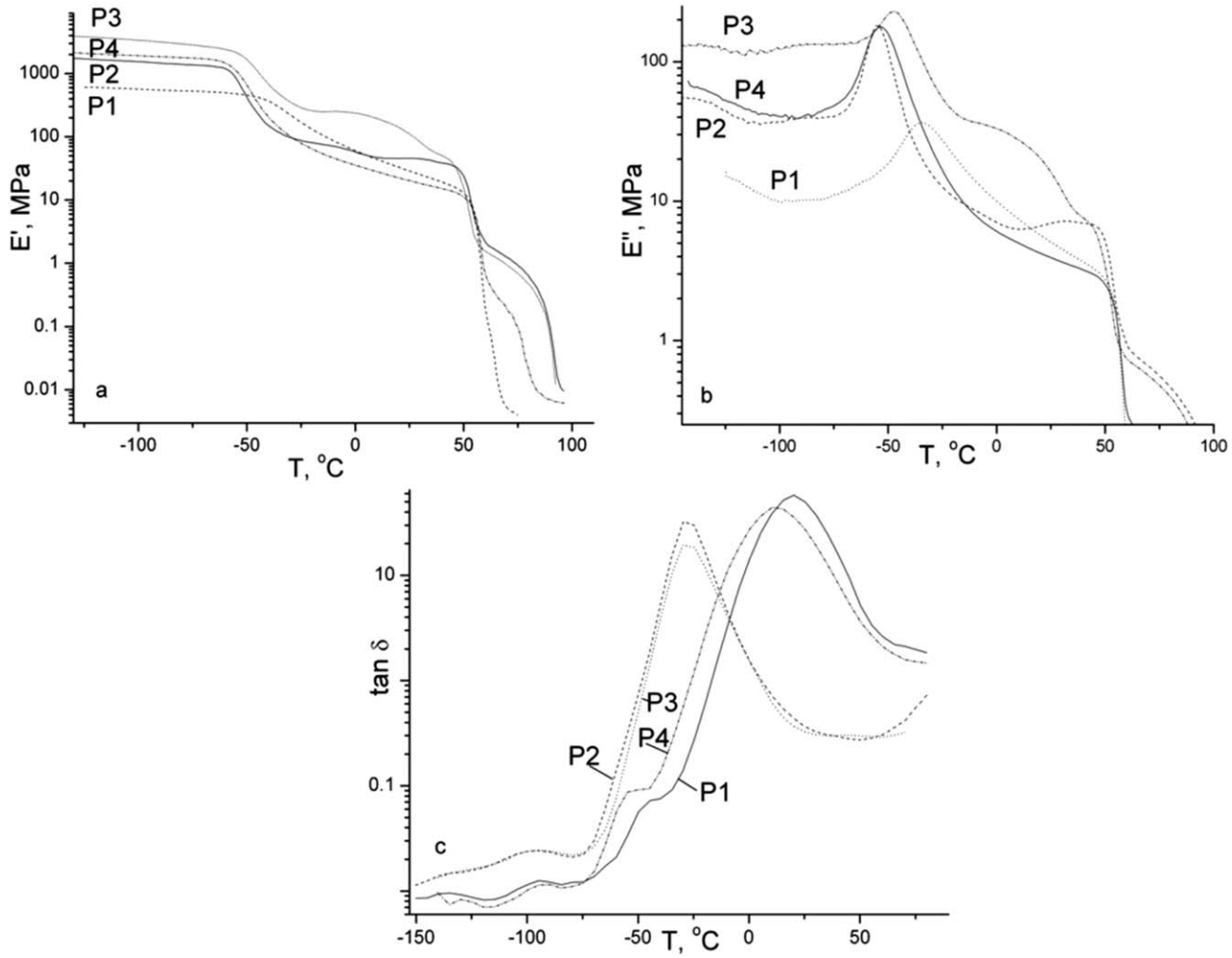

Figure 5. E′, E'', and tan δ as functions of the temperature at 1 Hz for the studied poly(ester ether)urethane ionomers.

strong conductivity relaxation peaks were observed. Semicrystalline polyurethanes can be expected to show strong interfacial polarization effects at temperatures above the glass transition. The sharp increase in the dielectric function was thought to be due to an interfacial or Maxwell–Wagner–Sillars polarization process caused by the trapping of the free charge carriers at the boundaries between the crystalline and amorphous regions.[36] In Figure 6(d), the isochronous curves (1 Hz) of the conductivities of P1–P4 are presented. Both the dipole relaxation time and the ionic conductivity are related to the T_g of a polymer. Static dipoles gain mobility during the glass transition and exhibit permittivity changes and dipole loss peaks. Charged ions also gain mobility as the polymeric material is heated through the glass transition and start to contribute to conductive losses above the glass transition. The contribution of the ion conductive loss to the measured loss factor can be huge and can shadow a small dipole loss contribution. Ionic conduction contributes in particular to the loss factor. For P1–P4, the conductivity (σ) curves showed identical behavior to the ε'' curves. As shown in Table IV, it was evident that the conductivity at RT for the studied polyurethanes increased in the following order: P1 < P4 < P2 < P3. The best conductivity was obtained for

Table IV. Transition Temperatures from the DMTA and DETA and Conductivity Values at RT (1 Hz) from DETA

Sample	$\alpha/\beta/\gamma$ (°C)[a]	$\alpha/\beta/\gamma$ (°C)[b]	σ at RT (1 Hz; S/cm)
P1	−34.3/−/−	−45.5/−79.4 (β');−93.5 (β)/−136.0	6.1E−9
P2	−55.1/−93.2/−136.5	−/−96.8/−135	7.4E−8
P3	−46.8/−89.0/−135	−/−97.6/−132	1.1E−7
P4	−54.0/−/−	−54.1/−93.7/−128	9E−9

[a] The α, β, and γ transitions were obtained from E'' of the DMTA curves.
[b] The α, β, and γ transitions were obtained from tan δ of the DETA curves.

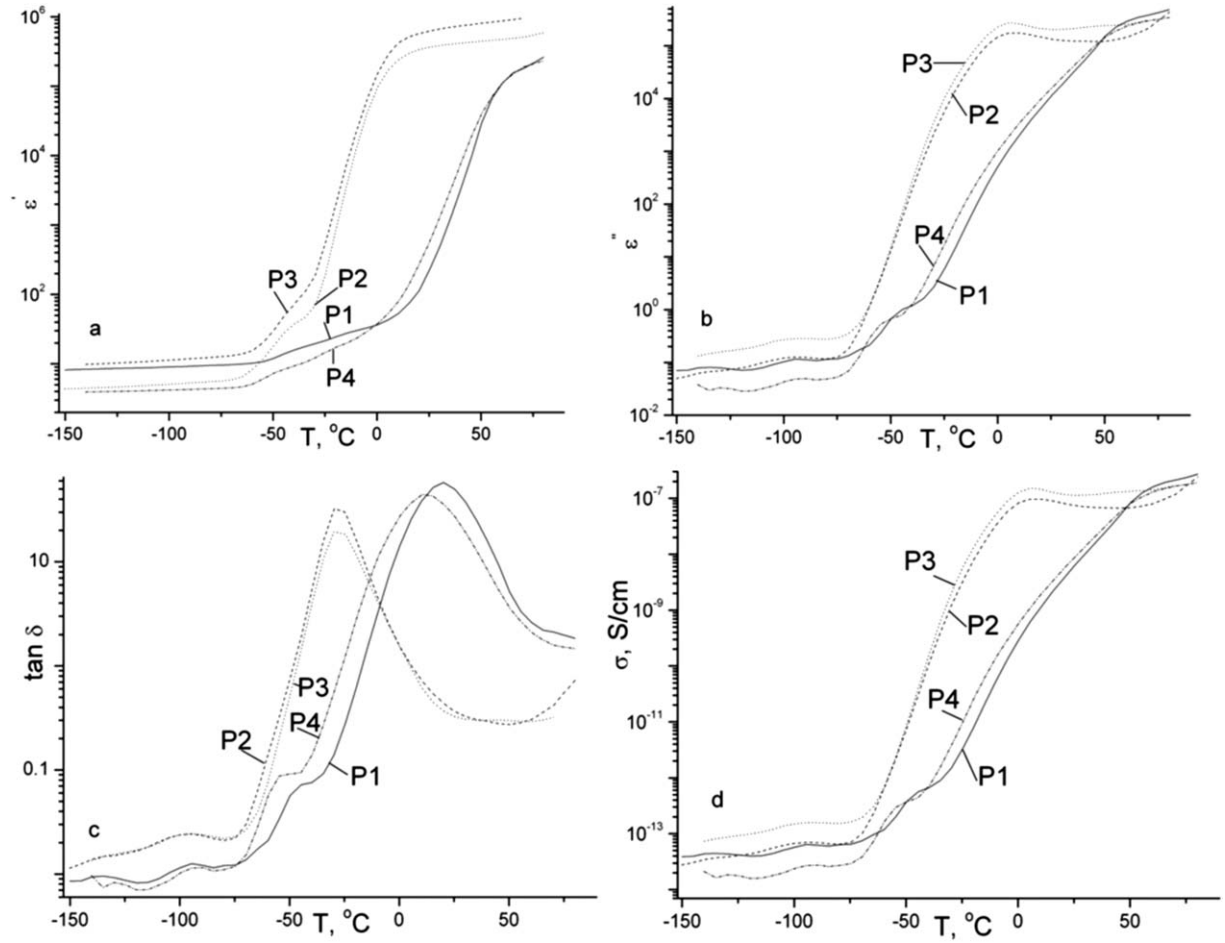

Figure 6. (a) Dielectric constant, (b) ε'', (c) tan δ, and (d) conductivity as functions of the temperature at 1 Hz for the studied poly(ester ether)urethane ionomers.

polyurethanes based on the PEO cosoft segment because of its high solvation capacity, especially of the cations. The ionic conductivity was strongly coupled to the polymer segmental relaxation. Usually, ions in polymer electrolytes associate into pairs and larger aggregates, and the ionic conductivity is determined by both the number of mobile charge carriers and their mobility. The cations are coordinated with abundant ether oxygens.

The dynamic relaxations observed in polymeric materials are time (f) dependent. As the perturbation f increases, it shifts the observed relaxations to higher temperatures. Figure 7 shows the

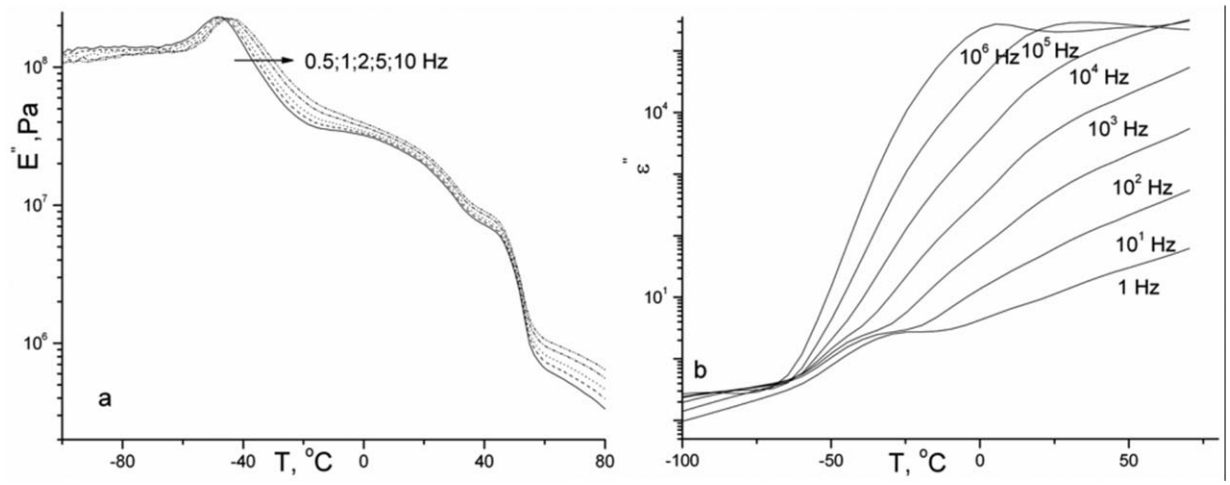

Figure 7. (a) E'' and (b) ε'' as functions of the temperature at different fs for the P3 polyurethane ionomer.

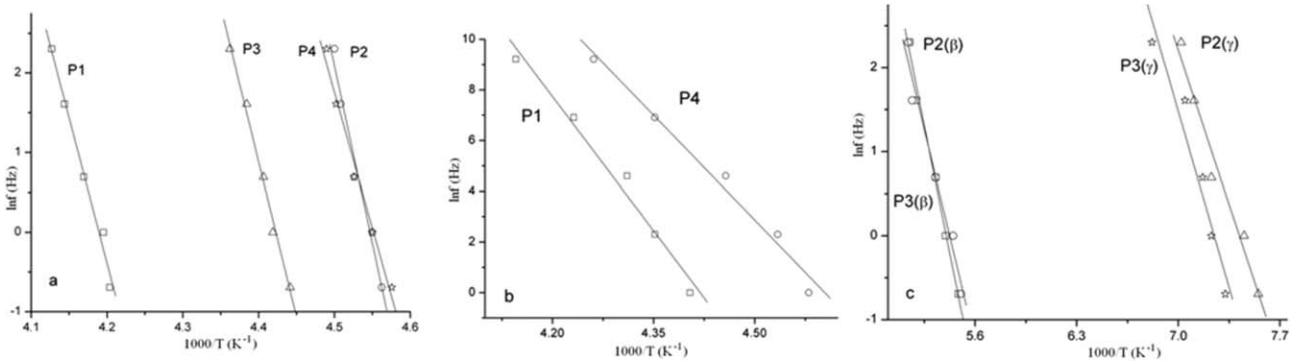

Figure 8. Arrhenius plots for the α, β, and γ transitions derived from the results of DMTA and DETA for the studied P1–P4 polyurethane ionomers: (a) α transition from DMTA (E'' vs temperature at various fs), (b) α transition from DETA (tan δ vs temperature at various fs), and (c) β and γ transitions from DMTA (E'' vs temperature at various fs).

dependence of E'' [Figure 7(a)] and ε'' [Figure 7(b)] on the temperature at different fs for polyurethane P3. From the E'' curves, it was evident that the glass-transition and secondary transition temperatures increased, and the corresponding moduli decreased with increasing f. From the ε'' curves, it was evident that the transitions were better revealed at lower fs. The multifrequency experiment indicated the α relaxation as an f-dependent process and the melting as an f-independent process [Figure 7(a)]. As shown in Figure 7(b), it was evident that large ε'' values occurred at higher fs in comparison with those occurring at lower temperatures when the chain segmental motion was practically frozen.

The glass and secondary relaxations were characterized by an Arrhenius-type temperature dependence of the relaxation times. Greater activation energy (E) values were found for more complex relaxations. With the relationship $f = (2\pi\tau)^{-1}$, where τ is relaxation time, a f value corresponded to each characteristic relaxation time, and an Arrhenius plot versus temperature was obtained. The data for the plot of ln f versus the the reciprocal temperature of transition were calculated as follows:

$$\ln f = \ln A - \left(\frac{E_a}{RT}\right)$$

where A is the pre-exponential factor, R is the gas constant, T is the temperature of transition, and E_a is the apparent activation energy.

In Figure 8, the plots of ln f versus the reciprocal temperature of transition for the studied polyurethanes P1–P4 with both the DMTA and DETA techniques are presented.

Table V. Values of E for the α, β, and γ Transitions Determined from the Results of DMTA and DETA for the Studied P1–P4 Polyurethanes

Sample	E_a from DMTA (kJ/mol)	E_a from DETA (kJ/mol)
P1	α: 303.4	α: 293.7
P2	α: 370.5; β: 72.0; γ: 43.6	–
P3	α: 324.1; β: 60.2; γ: 49.8	–
P4	α: 283.5	α: 229.2

Linear behavior was observed with the two methods, and E was determined. The values of E determined by the two methods are tabulated in Table V; they were found to be in line with those reported in the literature for polyurethanes.[23,37–39] The highest temperature or α process was the glass transition, which involved the cooperative motion of several molecular segments. Subglass β and γ relaxations take place in polymers either with or without flexible side groups and are believed to be produced by local rotational motions of the main chain and/or the motions of side groups with differing degrees of cooperativity and distribution of relaxation times. As reported in the literature, the secondary β relaxation was attributed to the local motions of polar urethane groups, the secondary β' relaxation was attributed to the movements of the cyclohexyl ring, and the secondary γ relaxation was attributed to the movements of the methylene sequences in the soft segments of the polyurethanes.[23,37–39]

Thermogravimetric Analysis

In this study, we aimed to evaluate the thermal stability and kinetic parameters of the investigated polyurethanes with TG and DTG under dynamic conditions of temperature. E, in terms

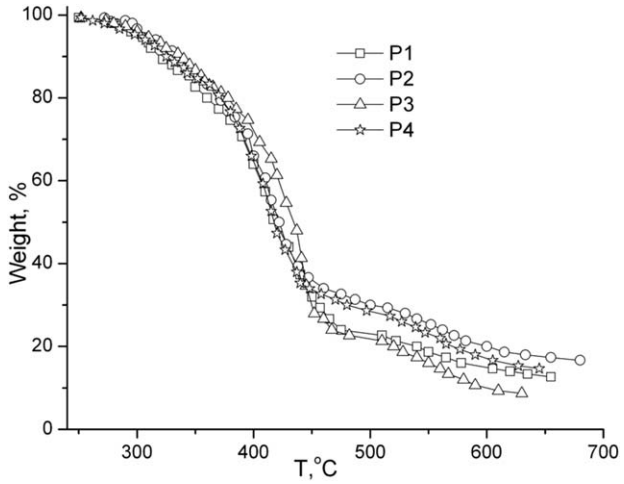

Figure 9. Thermogravimetric curves of the studied P1–P4 poly(ester ether)urethane ionomers.

Table VI. Thermal and Kinetic Characteristics of P1–P4 for Thermal Degradation Processes under Air

Sample	Main stage (°C)	wt %[a]	T_{max} (°C)	E (kJ/mol)	n
P1	215-500	76	325, 395	72.8	1.1
P2	215-487	68	320 (sh), 410	89.2	1.2
P3	215-510	79	330 (sh), 410	65.3	0.7
P4	217-500	71	350, 395	70.3	1.0

T_{max}, temperature corresponding to the maximum rate of decomposition.
[a] Weight loss percentage corresponding to the degradation stage.

of the Coats–Redfern[40] integral method, for the thermal degradation of the studied polyurethanes was estimated. The variation in the kinetic parameters with conversion was evaluated with the Reich–Levi method.[41] The thermogravimetric curves of the polyurethanes (P1–P4) are presented in Figure 9. The thermal characteristics obtained from the TG and DTG curves are tabulated in Table VI. Associated kinetic parameters, such as E and degradation order (n), of major importance in elucidating the mechanism of polymer degradation, were determined according to the Coats–Redfern method and are reported in Table VI.

The DTG thermograms showed at least three decomposition peaks for the studied polyurethanes P1–P4; these evidenced a multistage decomposition process in air. The multiple physicochemical processes involved in the degradation are, as a rule, lumped in one rate coefficient in the proposed mathematical models for thermal degradation derived from TG. The DTG curves of the polyurethanes P1–P4 displayed maximum peaks but also shoulder peaks. The stage of degradation of the polyurethanes at about 200–400°C was a result of the depolymerization of the urethane groups.[42–44]

Ether bonds are thermally labile and prone to oxidation.[45] The C—O bond is a weak bond in the macromolecular chain and, for that reason, is very susceptible to breaking down at low temperatures. The oxygen attack is initiated in the polyether flexible segment and, in most cases, occurs at the first carbon atom that attaches to the ether oxygen atom.[46] The evaluated kinetic parameters, E, and order of reaction by the applied Coats–Redfern integral method were related to the hard–soft segment morphology of the studied polyurethanes P1–P4. The estimated E represented a semiquantitative factor for characterizing the thermal stability. Usually, higher values of E are found for higher amounts of urethane groups, poly(ester urethane)s over poly (ether urethane)s, polyureas over polyurethanes, and Methylene Diphenyl Diisocyanate (MDI)-based polyurethanes over H_{12}MDI-based polyurethanes.[47–49] The values of E presented in Table VI fell between those found for poly(ether urethane)s and poly(ester urethane)s and corresponded to bisoft segments. E increased in the following order: P3 < P4 < P1 < P2. For the main stage of thermal degradation, polyurethane P3 evidenced the highest weight loss, the lowest E, and an order of reaction of less than 1; this suggested a prevalence of diffusion processes. Polyurethane P2 evidenced the lowest weight loss and the highest E and order of reaction. By determining the change in E as a function of conversion with the Levi–Reich kinetic analysis method, we compared the thermal decompositions of the studied poly(ester ether)urethane ionomers. The values of the reaction order estimated from the Coats–Redfern method (Table VI) were used in the calculation. The variation of E and the rate constant as functions of the conversion for the main degradation stages for P1–P4 are plotted in Figure 10.

It is evident from Figure 10(a) that in the initial stages of degradation, polyurethanes P1 and P2 showed distinct behavior in comparison with polyurethanes P3 and P4 because of the nature of random scission degradation of the C—O bonds of the ethylene oxide and propylene oxide segments in block and random structures. The initial stages of degradation are usually accompanied by weaker bonds, small molecular fragments forming into volatiles, and diffusion processes that are faster than chemical reactions. The plot with multiple peaks or inconstant Es indicated a multiple-step mass loss process. P3 and P4 showed an abrupt decrease up to conversion = 0.2, whereas P1 and P2 showed

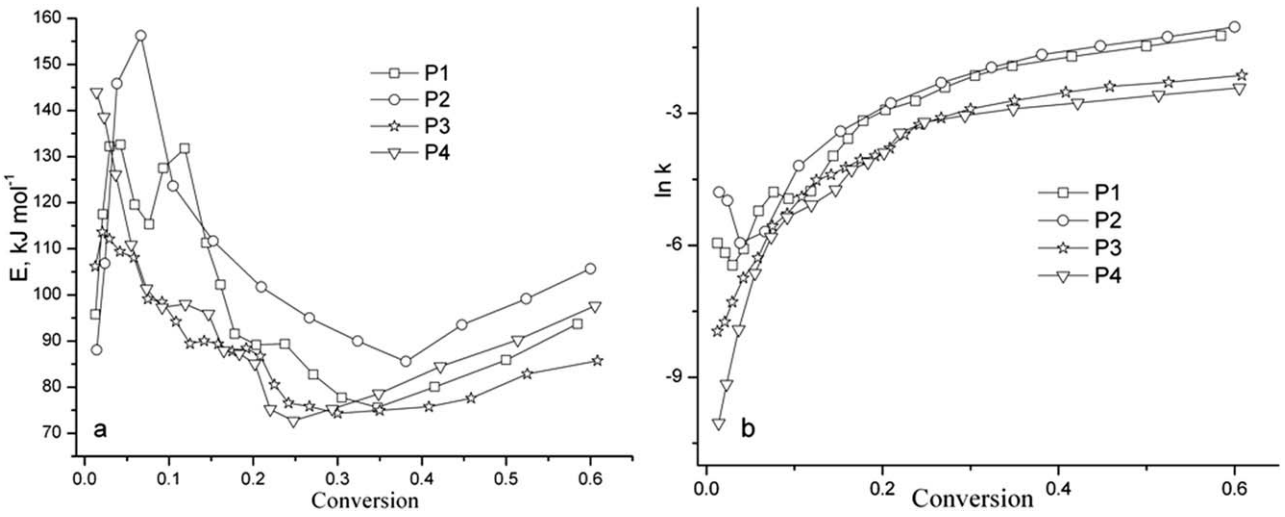

Figure 10. Variation of the (a) E and (b) rate constant (ln k) with conversion.

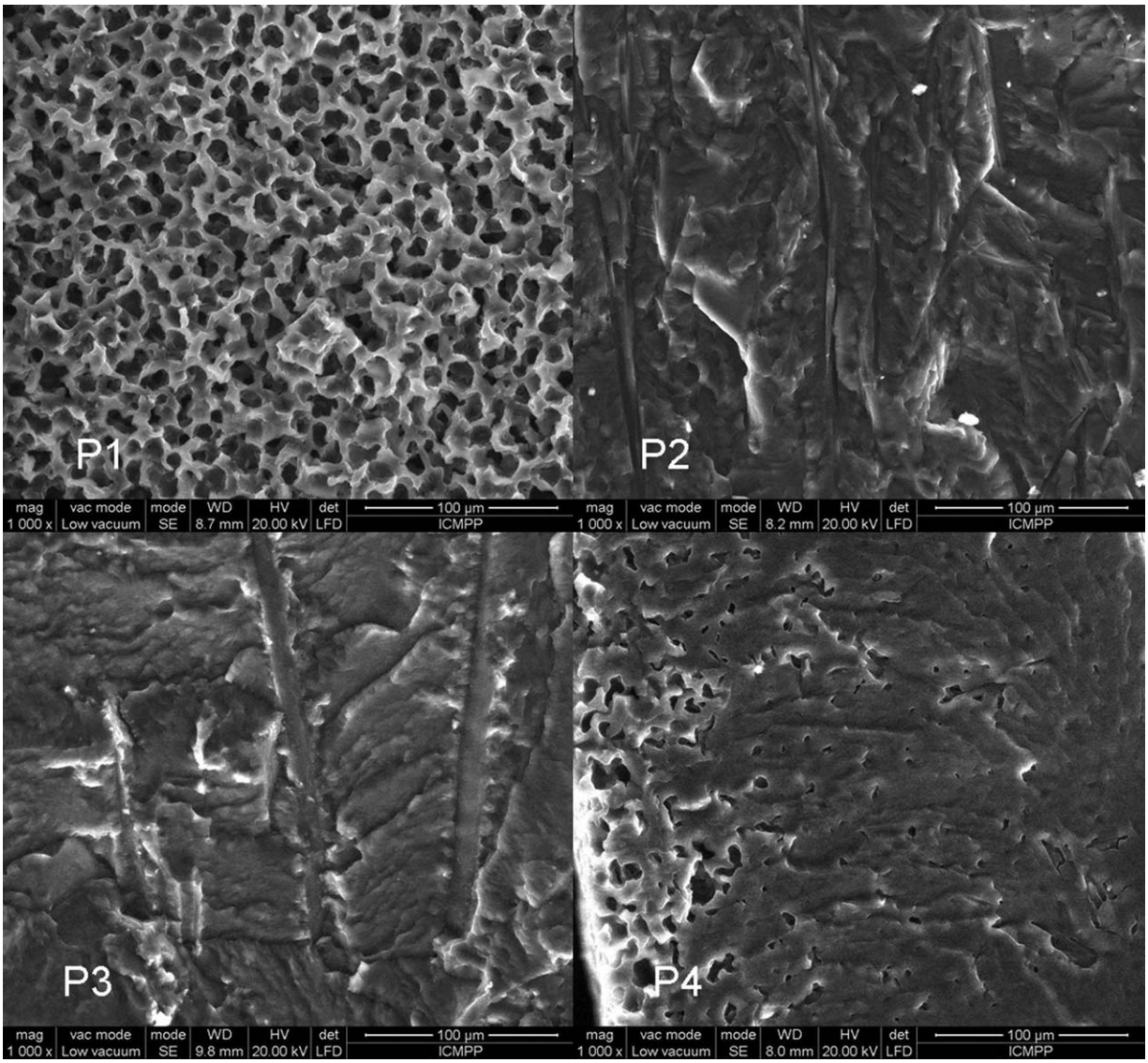

Figure 11. SEM micrographs (cross section) of the studied poly(ester ether)urethane ionomers.

abrupt increases in E at very low conversions. The increase in E with conversion was related to competitive reactions. After the decrease in E in the initial stage of degradation for P1–P4, E increased slightly up to conversion = 0.6; this proved that the stabilities of the intermediate products were rather similar. Reich–Levi curves showed E values in connection with the thermal stability; this was consistent with the order of P1–P4 determined by the Coats–Redfern integral method. It is obvious from Figure 10 that the behaviors of the rate constant and E were in agreement with the Arrhenius equation. For P1 and P2 at very low conversions, the rate constant decreased slightly with increasing conversion. It then increased slightly with increasing conversion and afterward tended to remain constant. For P3 and P4 at low conversions, the rate constant showed an increase with increasing conversion and afterward tended to remain constant.

SEM Analysis

In Figure 11, the SEM microphotographs (cross section) of the studied poly(ester ether)urethane ionomers P1–P4 are presented. They show distinctive behavior in terms of the morphology of the surface (cross section). The differences among the resulting phase-segregated morphologies of the polyurethane ionomers P1–P4 were due to different polyether cosoft segments with various PEO–PPO ratios; these influenced the supramolecular architecture, polyurethane hydrogen-bonding network, and specific ionic interactions between the SD moiety and polyether soft segments. The bulky bile-salt group affected the backbone conformation. It is known that bile acids are conformational responsive molecules because of the rigidity of their steroidal skeleton; this is a valuable asset for their supramolecular design and facial amphiphilic character. The bile-acid skeleton is curved when A and B units are in cis-fused configuration; this makes possible the formation of cavities, and it is specific to higher vertebrates, whereas in lower vertebrates, bile acid is flat because the A and B units are in a trans-fused configuration.[18] Bile-acid scaffolds are very well known in supramolecular chemistry. Because of their high levels of functionality, bile acids/salts

are exceptionally attractive for supramolecular chemistry in determining the translation of the molecular structure into function.

In case of polyurethane P1, a distinct three-dimensional scaffold morphology (size < 15 μm), namely, a microporous open cellular material with a high specific surface area for cell anchorage and a big volume for cell growth, migration, and effective fluid phase transport of nutrients, was obtained. Channeled porosity was remarked for the P2 (width < 10 μm) and P3 (width < 15 μm) samples. Stronger ionic interactions as in the case of P2, the P3 samples had more close-packed and compact structures. For the P4 sample, randomly distributed individual micropores of irregular shape with through and nonthrough character (size < 15 μm) were observed.

CONCLUSIONS

New SD-based poly(ester ether)urethane ionomer biomembranes intended for biomedical applications are presented. Calorimetric, dynamic mechanical, and dielectric measurements were performed to delineate the types and dynamic rates of molecular scale motion in the polyurethane supramolecular networks. The T_g values calculated with DMTA and DETA techniques were found to be higher than those obtained with DSC. Changes in the thermomechanical properties of a given material are usually more dramatic than Δcp's, and therefore, the sensitivity of DSC is usually not good enough and overlaps thermal events related to the pure phases and interphases. The results of the main and secondary transition temperature values and the corresponding E values determined with the DMTA and DETA techniques supported each other well. The thermal stability and kinetic parameters of the investigated polyurethanes with TG and DTG under dynamic conditions of temperature in air were determined. We found that for the main stage of thermal degradation, the values of E fell between those found for poly(ether urethane)s and poly(ester urethane)s and corresponded to the bisoft segments. The differences in the supramolecular organization of the hydrogen-bonding network, molecular dynamics, conductivity, ionic interactions, morphology of biomembranes, and conformational interaction of the rigid steroid skeleton within the polyurethane matrix were dictated by the ratio between the PEO segments and PPO segments in these polyurethanes. Higher conductivities, stronger ionic interactions, and a higher solvation capacity of ions were found for PEO-rich segments of the polyurethanes than in the PPO-rich segment of the polyurethanes. A distinct three-dimensional scaffold morphology was obtained in case of the Pluronic L31-based P1.

ACKNOWLEDGMENTS

The authors gratefully acknowledge the financial support given by Unitatea Executiva pentru Finantarea Invatamantului Superior, a Cercetarii, Dezvoltarii si Inovarii through the research project BIONANOMED 164/2012.

REFERENCES

1. Lelah, M. D.; Cooper, S. L. Polyurethanes in Medicine; CRC: Boca Raton, FL, **1993**.
2. Plank, H.; Syre, I.; Dauner, M.; Egberg, G. Polyurethanes in Biomedical Engineering II: Proceedings of the 2nd International Conference on Polyurethanes in Biomedical Engineering; Progress in Biomedical Engineering 3; Elsevier Applied Science: Amsterdam, **1987**.
3. Vermette, P. Biomedical Applications of Polyurethanes; Tissue Engineering Intelligence Unit 6; Eurekah.com/Landes Bioscience: Georgetown, TX, **2001**.
4. Macocinschi, D.; Filip, D.; Vlad, S. *Polym. Compos.* **2010**, *31*, 1956.
5. Lan, P. N.; Corneillie, S.; Schacht, E.; Davies, M.; Shard, A. *Biomaterials* **1996**, *17*, 2273.
6. Wang, N.; Burugapalli, K.; Wijesuriya, S.; Far, M. Y.; Song, W.; Moussy, F.; Zheng, Y.; Ma, Y.; Wu, Z.; Li, K. *Biofabrication* **2014**, *6*, 015002.
7. Jozwiak, A. B.; Kielty, C. M.; Black, R. A. *J. Mater. Chem.* **2008**, *18*, 2240.
8. Lamba, N. M. K.; Woodhouse, K. A.; Cooper, S. L. Polyurethanes in Biomedical Applications; CRC: Boca Raton, FL, **1998**.
9. Yu, L. Biodegradable Polymer Blends and Composites from Renewable Resources; Wiley: Hoboken, NJ, **2009**.
10. Kaali, P.; Stromberg, E.; Aune, R. E.; Czel, G.; Momcilovic, D.; Karlsson, S. *Polym. Degrad. Stab.* **2010**, *95*, 1456.
11. Romero, M. R.; Martinez-Diez, M. C.; Larena, M. G.; Macias, R. I. R.; Dominguez, M.; Garcia-Monzon, C.; Serrano, M. A.; Marin, J. J. G. *Antivir. Chem. Chemother.* **2002**, *13*, 371.
12. Gautrot, J. E.; Zhu, X. X. J. *Biomater. Sci. Polym. Ed.* **2006**, *17*, 1123.
13. Zuluaga, F.; Valderruten, N. E.; Wagener, K. B. *Polym. Bull.* **1999**, *42*, 41.
14. Gouin, S.; Zhu, X. X.; Lehnert, S. *Macromolecules* **2000**, *33*, 5379.
15. Melia, E.; Haddleton, D. M. *Polym. Prepr.* **2005**, *46*, 166.
16. Gautrot, J. E.; Zhu, X. X. *Angew. Chem. Int. Ed.* **2006**, *45*, 6872.
17. Janvier, F.; Zhu, J. X. X.; Armstrong, J.; Meiselman, H. J.; Cloutier, G. *J. Mech. Behav. Biomed.* **2013**, *18*, 100.
18. Zhang, J. W.; Zhu, X. X. *Sci. China Ser. B* **2009**, *52*, 849.
19. Nelson, A. M.; Long, T. E. *Macromol. Chem. Phys.* **2014**, *215*, 2161.
20. Zhu, W.; Wang, X.; Yang, B.; Wang, L.; Tang, X.; Yang, C. J. *Mater. Sci.* **2001**, *36*, 5137.
21. Buruiana, T.; Buruiana, E. C. J. *Appl. Polym. Sci.* **2002**, *86*, 1240.
22. Musteata, V. E.; Filip, D.; Vlad, S.; Macocinschi, D. *Opt. Adv. Mater. Rapid Commun.* **2010**, *4*, 1187.
23. Macocinschi, D.; Filip, D.; Vlad, S.; Cristea, M.; Musteata, V.; Ibanescu, S. *J. Biomater. Appl.* **2010**, *27*, 119.
24. Chang, C.-C.; Chen, K.-S.; Yu, T. L.; Chen, Y.-S.; Tsai, C.-L.; Tseng, Y.-H. *Polym. J.* **1999**, *31*, 1205.
25. Marcos-Fernandez, A.; Lozano, A. E.; Gonzales, L.; Rodriguez, A. *Macromolecules* **1997**, *30*, 3584.
26. Yılgor, E.; Yılgor, I.; Yurtsever, E. *Polymer* **2002**, *43*, 6551.

27. Mattia, J.; Painter, P. A. *Macromolecules* **2007**, *40*, 1546.
28. Struszczyk, H. *J. Macromol. Sci.* **1986**, *23*, 973.
29. Pimentel, G. C.; Sederholm, C. H. *J. Chem. Phys.* **1956**, *24*, 639.
30. Iyer, S.; Schiraldi, D. A. J. *Polym. Sci. Part B: Polym. Phys.* **2006**, *44*, 2091.
31. Cristea, M.; Ionita, D.; Simionescu, B. C. *Eur. Polym. J.* **2010**, *46*, 2005.
32. Korley, L. T. J.; Pate, B. D.; Thomas, E. L.; Hammond, P. T. *Polymer* **2006**, *47*, 3073.
33. Waletzko, R. S.; Korley, L. T. J.; Pate, B. D.; Thomas, E. L.; Hammond, P. T. *Macromolecules* **2009**, *42*, 2041.
34. Maurya, K. K.; Srivastava, N.; Hashmi, S. A.; Chandra, S. *J. Mater. Sci.* **1992**, *27*, 6357.
35. Mohsen, N. M.; Craig, R. G.; Filisko, F. E. *J. Oral Rehabil.* **2001**, *28*, 376.
36. Kremer, F.; Schonhals, A. Broadband Dielectric Spectroscopy; Springer: Berlin, **2003**.
37. Sekkar, V.; Bhagawan, S. S.; Prabhakaran, N.; Rama Rao, M.; Ninan, K. N. *Polymer* **2000**, *41*, 6773.
38. Okrasa, L.; Czech, P.; Boiteux, G.; Mechin, F.; Ulanski, J. *Polymer* **2008**, *49*, 2662.
39. Fragiadakis, D.; Runt, J. *Macromolecules* **2013**, *46*, 4184.
40. Coats, A. W.; Redfern, J. T. *Nature* **1964**, *201*, 68.
41. Reich, L.; Levi, D. W. *Makromol. Chem.* **1963**, *66*, 102.
42. Saunders, J. H. *Rubber Chem. Technol.* **1959**, *32*, 337.
43. Petrovic, Z. S.; Zavargo, Z.; Flynn, J. H.; Macknight, W. J. J. *Appl. Polym. Sci.* **1994**, *51*, 1087.
44. Monteavaro, L. L.; Riegel, I. C.; Petzhold, C. L.; Samios, D. *Polimeros* **2005**, *15*, 151.
45. Singh, A.; Weissbein, L.; Mollica, J. C. *Rubber Chem. Technol.* **1969**, *42*, 648.
46. Gallet, G.; Carroccio, S.; Rizzarelli, P.; Karlsson, S. *Polymer* **2002**, *43*, 1081.
47. Filip, D.; Macocinschi, D.; Gradinaru, L. M. *Polym. Degrad. Stab.* **2013**, *98*, 951.
48. Filip, D.; Macocinschi, D.; Vlad, S. *Compos. B* **2011**, *42*, 1474.
49. Filip, D.; Macocinschi, D.; Ioanid, G. E.; Vlad, S. *Polimery* **2010**, *55*, 358.